Robust Target Positioning for Reconfigurable Intelligent Surface Assisted MIMO Radar Systems

Zhen Chen, *Senior Member, IEEE,* Jie Tang, *Senior Member, IEEE,* Lei Huang, *Senior Member, IEEE,* Zhen-Qing He, Kai-Kit Wong, *Fellow, IEEE* and Jiangzhou Wang, *Fellow, IEEE*

***Abstract*—The direction of arrival (DOA) based multiple-input multiple-output (MIMO) radar technique has been widely utilized for ubiquitous positioning due to its advantage of simple implementability. On the other hand, reconfigurable intelligent surface (RIS) has received considerable attention, which can be deployed on the walls and objects to strengthen the positioning performance. However, RIS is usually not equipped with a perception module, which results in the tremendous challenge for RIS-assisted positioning. To tackle this challenge, this paper propose the fundamental problem of DOA-based target positioning in RIS-assisted MIMO radar system. Unlike conventional DOA estimation systems, the beneficial role of RIS is investigated in MIMO radar system, where a nonconvex ℓ_p promoting function is exploited to estimate DOA task. By adjusting the reflecting elements of the RIS, the proximal projection iterative strategy is developed to obtain the feasible solution. Both theoretical analysis and simulation results illustrate that the proposed scheme can achieve remarkable positioning performance and shed light on the benefits offered by the adoption of the RIS in terms of positioning performance.**

This work has been supported in part by National Key Research and Development Program of China under Grant 2019YFB1804100, in part by the National Natural Science Foundation of China under Grant 62001171, 61971194, 62222105, in part by the Engineering and Physical Sciences Research Council (EPSRC) under grant EP/V052942/1, in part by the National Science Fund for Distinguished Young Scholars under Grant 61925108, in part by the Key Project of International Cooperation and Exchanges of the National Natural Science Foundation of China under Grant 62220106009, in part by the Natural Science Foundation of Guangdong Province under Grant 2021A1515011966, 2022A1515011189, the project of Shenzhen Peacock Plan Teams under Grant KQTD20210811090051046, in part by the Special Project for Guangxi Science and Technology Bases and Talents under Grant AD21075054, in part by the Open Research Fund of Guangdong Key Laboratory of Aerospace Communication and Networking Technology under Grant 2018B030322004, in part by the Open Research Fund of State Key Laboratory of Integrated Services Networks, Xidian University under Grant ISN23-05, in part by the Research Fund of Guangxi Key Lab of Multi-source Information Mining and Security under grant MIMS22-05, in part by the Natural Science Foundation of Sichuan Province under grant 2022NSFSC0880 and in part by the International Science and Technology Cooperation Project of Guangzhou (Huangpu) under Grant 2020GH06. (*Corresponding author: Jie Tang, Lei Huang*.)

Z. Chen is with the School of Electronic and Information Engineering, Shenzhen University, Shenzhen, China, and also with the State Key Laboratory of Integrated Services Networks, Xidian University, Xian, China (e-mail:chenz.scut@gmail.com).

J. Tang is with the School of Electronic and Information Engineering, South China University of Technology, Guangzhou, China (e-mail:eejtang@scut.edu.cn).

L. Huang is with the State Key Laboratory of Radio Frequency Heterogeneous Integration (Shenzhen University), Shenzhen 518060, China (e-mail: lhuang@szu.edu.cn).

Z.-Q. He is with the School of Aeronautics and Astronautics, Sichuan University, Chengdu 610065, China (e-mail: zhenqinghe@scu.edu.cn)

K.-K Wong is with the Department of Electronic and Electrical Engineering, University College London, London, United Kingdom. (e-mail: kaikit.wong@ucl.ac.uk).

J. Wang is with the School of Engineering and Digital Arts, University of Kent, Canterbury, U.K. (e-mail: j.z.wang@kent.ac.uk).

***Index Terms*—Alternative minimization, MIMO radar, DoA estimation, Target positioning**

I. Introduction

MULTIPLE-input multiple-output (MIMO) radar has received considerable attention because it can achieve significantly enhanced target positioning and parameter estimation performance through utilizing the waveforms spatial diversity [1]. Unlike the conventional phased array radar (PAR), MIMO radar systems is equipped with multiple antennas to transmit/receive multiple independent (orthogonal) waveforms using radar cross section (RCS) diversity [2]. Therefore, the MIMO radar can offer better parameter identifiability, resolution and robustness against correlated sources, which is superior to the PAR approach. It was confirmed that MIMO radar systems can offer considerable advantages over conventional phased-array radars in various aspects of MIMO radar system [2]–[4], especially in the estimation of target positioning parameters, such as time-of-arrival (TOA) [3], and direction of arrival (DOA) [4]. Among various kinds of positioning techniques, DOA-based technique is one of the most fundamental topics because it can be easily implemented on the MIMO radar systems with little hardware requirements. For example, [4] investigated a tensor decomposition-based DOA estimation for transmit beamspace MIMO radar, where the Vandermonde structure of the factor matrix was exploited to estimate the phase rotations. Since Bartlett beamformer has low computational complexity, Bartlett-absed techniques were introduced to DOA estimation with arbitrary array structure [5]. Besides, multiple signal classification (MUSIC) was also developed for DOA estimation [6]–[8]. Compared with the Bartlett, MUSIC offering a much better resolution, which is one of the most popular techniques [8]. In addition, a sparse representation framework also was exploited to provide the desired DOA resolution in the high-resolution target positioning scenario [9]. The iterative procedure is performed well only when the sparsity of signals is known.

More recently, reconfigurable intelligent surface (RIS) has significant advantages in terms of expanding signal coverage and reducing deployment and energy costs [10], [11]. RIS can intelligently control the incident signal to transmit the data through adjusting its the reflection elements [12]. Compared with conventional relays, RIS provides low hardware footprints and noises would not be magnified during signal transmission [13]. Consequently, RIS has received widespread attention in the literature. Inspired by the freedom offered by RIS to

Fig. 1: A RIS-assisted MIMO radar positioning.

manipulate transmitted signals, researchers have been investigated the RIS-assisted DOA estimation benefits for target localization of MIMO radar systems [14]. Subsequently, an architecture of joint positioning and communication scheme was developed, which employed an hierarchical codebooks-based RIS design and feedback from the mobile station [15]. In addition, RIS was also employed to joint communication and achievable localization, where closed-form RIS phase profile is designed for various localization scenarios. In practical scenarios, signals contain unknown noise, e.g., traffic/electric noise, which leads to serious positioning resolution degradation because of the incorrect white Gaussian noise assumption [16]. It is obvious that an ideal estimator should be robust to the ubiquitous noise in practical engineering applications.

In this paper, robust target positioning for RIS-assisted MIMO radar system is investigated to enhance the positioning resolution. The main contributions can be summarized as follow:

- We consider a robust ℓ_p model to estimate DOA-based target positioning, where the low-cost RIS is used to provide a strong LoS environment, which is beneficial for improving positioning performance.
- To solve highly intractable nonconvex problem, the formulated problem is transformed equivalently into the reweighted ℓ_2 problem, where the phase shifts design for the RIS is derived to enhance the positioning performance by exploiting proximal projection approach.
- Two regularization parameters are exploited to adaptively control the noise intensity, and, through numerical analysis, the superiority and effectiveness of the proposed approach is verified to achieve centimeter-level positioning accuracy.

II. System Model

Considering a RIS-assisted MIMO radar system, the transmitter and receiver are equipped with M and N closely-spaced elements, respectively. RIS takes the form of a uniform planar array (UPA) and consists of L reflecting elements, which is controlled by the receiver, as shown in Fig. 1. We define $L = L_x \times L_y$, where L_x is the number of row elements and L_y is the number of column elements. The phase shifts of RIS can be tuned to help the radar transmitter/receiver illuminating the prospective target.

The signals at the receiver are comprised of two paths: from the target to RIS, from RIS to the radar receiver, as described in Fig. 1. From [2], we define the transmit-receive steering matrix as

$$\boldsymbol{A}(\theta) \triangleq \boldsymbol{a}_t(\theta_t)\boldsymbol{a}_r^T(\theta_r) = \underbrace{\vartheta_r \boldsymbol{\Gamma}_r \boldsymbol{\Theta}_r \boldsymbol{w}_r}_{R\to\mathrm{RIS}\to T} \underbrace{\boldsymbol{w}_t^T \boldsymbol{\Theta}_t \boldsymbol{\Gamma}_t^T \vartheta_t}_{T\to\mathrm{RIS}\to R}, \tag{1}$$

where ϑ_t is the indirect channels from the transmit element to the RIS's reflecting element to the target, which represents the radar element gain, the array coefficients of the bistatic radar cross-section (RCS), the two-hop path-loss and phase delay. ϑ_r is the indirect channels from the target to the RIS's reflecting coefficients to the receiver. $\boldsymbol{\Gamma}_t$ is the normalized channel matrices from the radar transmitter to the RIS, whose entries account for the gain of the radar, the reflecting element of the bistatic RCS, the multi-path fading and the phase delay; $\boldsymbol{\Gamma}_r$ is the normalized channel matrices from the RIS to the radar receiver. $\boldsymbol{\Theta}_t = \mathrm{diag}\{e^{j\psi_{t,1}}, ..., e^{j\psi_{t,N}}\}$ and $\boldsymbol{\Theta}_r = \mathrm{diag}\{e^{j\psi_{r,1}}, ..., e^{j\psi_{r,N}}\}$ are the forward and backward reflecting response of RIS, respectively. $\boldsymbol{w}_t$ and $\boldsymbol{w}_r$ denote the direct steering vectors of the radar transmitter and receiver towards the directions θ_t and θ_r of the target, respectively. Notice that $\boldsymbol{a}_t(\theta)$ and $\boldsymbol{a}_r(\theta)$ is defined as the indirect transmit and receive steering vectors of the radar towards the target, respectively, where RIS is designed to determine its direction.

The signal received from a single target, in far-field with constant radial velocity at an angle θ can be written as

$$\begin{aligned}\mathbf{z} &= \alpha e^{-j\varsigma_c t}\mathrm{vec}(\boldsymbol{A}(\theta)) + \boldsymbol{\varepsilon} \\ &= \alpha e^{-j\varsigma_c t}(\vartheta_t \boldsymbol{\Gamma}_t^H \otimes \boldsymbol{\Gamma}_r \vartheta_r)\left(\boldsymbol{\Theta}_t^T \otimes \boldsymbol{\Theta}_r\right)\mathrm{vec}\left(\boldsymbol{w}_r \boldsymbol{w}_t^T\right) + \boldsymbol{\varepsilon},\end{aligned} \tag{2}$$

where α denotes the unknown target response and any other scaling factor not included in the target signature, and $\boldsymbol{\varepsilon} = \ddot{\boldsymbol{e}} + \boldsymbol{e}$, where $\ddot{\boldsymbol{e}}$ denotes a large amplitude of the unwarranted interference or the impulsive noise, $\boldsymbol{e}$ denotes the dense noise. $\otimes$ denotes the Kronecker product.

To promote a feasible solution, we discretize the target state space into a grid of possible values L. Thus, the target is associated with a state vector belonging to this grid, which contribute to the matched filter output. To this end, When a target $\{\alpha^l, \forall l = 1, ..., L\}$ are present, we define $\boldsymbol{\Phi}_l(\varphi) \triangleq \alpha^l(\vartheta_t \boldsymbol{\Gamma}_t^H \otimes \boldsymbol{\Gamma}_r \vartheta_r)\left(\boldsymbol{\Theta}_t^T \otimes \boldsymbol{\Theta}_r\right)$. Also, if α^l is the state vector of the target, we define $\boldsymbol{\vartheta}_l = \mathrm{vec}\left(\boldsymbol{w}_r \boldsymbol{w}_t^T\right)$, Otherwise, $\boldsymbol{\vartheta}_l = \mathbf{0}$. Finally, stacking $\{\boldsymbol{\Phi}_l(\varphi)\}_{l=1}^L$ and $\{\boldsymbol{\vartheta}_l\}_{l=1}^L$ into a high-dimensional column vector and the matrix, respectively, we have

$$\begin{aligned}\boldsymbol{\Phi}(\boldsymbol{\varphi}) &= \left[\boldsymbol{\Phi}_1(\varphi), ..., \boldsymbol{\Phi}_l(\varphi), ..., \boldsymbol{\Phi}_L(\varphi)\right], \\ \boldsymbol{\vartheta} &= \left[\boldsymbol{\vartheta}_1^T, ..., \boldsymbol{\vartheta}_l^T, ..., \boldsymbol{\vartheta}_L^T\right]^T.\end{aligned} \tag{3}$$

After compensating the range-Doppler parameters, we can simplify equation (2) as

$$\mathbf{z} = \boldsymbol{\Phi}(\boldsymbol{\varphi})\boldsymbol{\vartheta} + \boldsymbol{\varepsilon}. \tag{4}$$

For the system model (4), our aim is to estimate the direction $\boldsymbol{\theta}$ of target and phase shifts $\boldsymbol{\varphi}$ of RIS. Thus, we consider

the sparsity-regularization model, which is formulated as

$$\min_{\boldsymbol{\vartheta},\boldsymbol{\varphi}} \frac{1}{2}\left\|\mathbf{z}-\boldsymbol{\Phi}(\boldsymbol{\varphi})\boldsymbol{\vartheta}\right\|_p^p + \lambda\sum_{i=1}^{N} g(\vartheta_i), \tag{5}$$

where λ is the regularization parameter that to be selection properly. $g(\vartheta_i) \triangleq \log(|\vartheta_i|^2+\delta)$ with $\delta > 0$ is a sparsity-encouraging function.

According to the theory of compressed sensing [17] that the ℓ_p-norm penalty criterion with $p = 2$ has attracted extensive attention since they are easy to be implemented in Gaussian noise. However, this rapidly increasing ℓ_2 penalty may not suitable to characterize noise-specific errors, such as impulsive noise. Thus, a natural modification was suggested for the $p < 2$, and the following weighted formulation is employed for the target positioning:

$$\min_{\boldsymbol{\vartheta},\boldsymbol{\varphi}} \left\{ Q(\boldsymbol{\vartheta},\boldsymbol{\varphi}) \triangleq \frac{1}{2}\sum_{m=1}^{M}\omega_\mu^p\left([\mathbf{z}-\boldsymbol{\Phi}(\boldsymbol{\varphi})\boldsymbol{\vartheta}]_m\right) + \lambda\sum_{i=1}^{N} g(\vartheta_i)\right\}, \tag{6}$$

where $\omega_\mu^p(x)$ is defined as

$$\omega_\mu^p(x) \triangleq \begin{cases} \dfrac{p}{2}\mu^{p-2}|x|^2, & |x| \le \mu \\ |x|^p - \dfrac{2-p}{2}\mu^p, & |x| > \mu \end{cases} \tag{7}$$

From [17], the penalty term $\omega_\mu^p(x)$ with generalized $\ell_p (0 < p \le 2)$ is a smoothed approximation function of $|x|^p$ around the nonsmoothed term $|x| = 0$. Obviously, the formulated optimization problem (6) obtains a more generalized forms because considering $\omega_\mu^p(x)$ as a fitting metric to suppress the various type of noises is essentially twofold. First, in practical applications, the parameters μ and p can be adjusted for various type of noises. Second, it is computationally tractable due to its continuity and differentiability. Therefore, the ℓ_p-norm based data-fidelity fitting criterion is less sensitive to outliers with abnormal noise.

III. Robust DOA Estimation for RIS-assisted Radar System

The optimization problem (6) is known to be an NP-hard problem. To solve the resulting non-convex problem, a proximal iteratively approximation ℓ_p scheme is proposed by employing the majorization-minimization (MM) framework. Before deriving the proposed approach, the useful lemma is introduced to design the ℓ_p surrogate function.

Lemma 1. *[18] Given $\mu > 0$ and $0 < p < 2$, the following inequalities hold:*

$$\omega_\mu^p(s) \le \tilde{\omega}_\mu^p(s,\tilde{s}) \triangleq \frac{p}{2}|s|^2|\eta|^{p-2} + \frac{2-p}{2}(|\eta|^p - \mu^p) \tag{8}$$

where

$$\eta = \begin{cases} \mu, & |\tilde{s}| \le \mu \\ |\tilde{s}|, & |\tilde{s}| > \mu \end{cases}, \quad \forall s,\tilde{s} \in \mathbb{C} \tag{9}$$

with equality achieved at $s = \tilde{s}$.

According to Lemma 1, the upper bound of $g(\vartheta_i)$ and $\omega_\mu^p\left([\mathbf{z}-\boldsymbol{\Phi}(\boldsymbol{\varphi})\boldsymbol{\vartheta}]_m\right)$ can be equivalently represented by

$$g(\vartheta_i) \le \tilde{g}(\vartheta_i,\vartheta_i^{(k)}) \triangleq \frac{|\vartheta_i|^2}{|\vartheta_i^{(k)}|+\zeta} + C \tag{10}$$

and

$$\begin{aligned}\omega_\mu^p\left([\mathbf{z}-\boldsymbol{\Phi}(\boldsymbol{\varphi})\boldsymbol{\vartheta}]_m\right) &\le \tilde{\omega}_\mu^p\left([\mathbf{z}-\boldsymbol{\Phi}(\boldsymbol{\varphi})\boldsymbol{\vartheta}]_m, [\mathbf{z}-\boldsymbol{\Phi}(\boldsymbol{\varphi})\boldsymbol{\vartheta}^{(k)}]_m\right) \\ &\triangleq \eta_m\left|[\mathbf{z}-\boldsymbol{\Phi}(\boldsymbol{\varphi})\boldsymbol{\vartheta}]_m\right|^2 + C\end{aligned} \tag{11}$$

where $\boldsymbol{\beta}^{(k)} \triangleq [\beta_1^{(k)},...,\beta_n^{(k)},...,\beta_N^{(k)}]^T$ represents kth iteration result of $\boldsymbol{\beta}$ and

$$\eta_m(\boldsymbol{\varphi}) = \begin{cases} \dfrac{p}{2}\mu^{p-2}, & \left|\left[\mathbf{z}-\boldsymbol{\Phi}(\boldsymbol{\varphi})\boldsymbol{\vartheta}^{(k)}\right]_m\right| \le \mu \\ \dfrac{p}{2}\left|\left[\mathbf{z}-\boldsymbol{\Phi}(\boldsymbol{\varphi})\boldsymbol{\vartheta}^{(k)}\right]_m\right|^{p-2}, & \left|\left[\mathbf{z}-\boldsymbol{\Phi}(\boldsymbol{\varphi})\boldsymbol{\vartheta}^{(k)}\right]_m\right| > \mu \end{cases} \tag{12}$$

It follows that the equations in (10) and (11) will be held at $\beta_i = \beta_i^{(k)}$ $i = 1,...,N$, respectively. Furthermore, combining (10) with (11), the objective function in (6) can be majorized by the following weighted surrogate function:

$$\begin{aligned}Q(\boldsymbol{\vartheta},\boldsymbol{\varphi},\boldsymbol{\vartheta}^{(k)}) \triangleq &\boldsymbol{\beta}^H\boldsymbol{\Upsilon}^{(k)}\boldsymbol{\beta} + \lambda^{-1}\left[\mathbf{z}-\boldsymbol{\Phi}(\boldsymbol{\varphi})\boldsymbol{\vartheta}\right]^H \\ &\times\boldsymbol{\eta}^{(k)}(\boldsymbol{\varphi})\left[\mathbf{z}-\boldsymbol{\Phi}(\boldsymbol{\varphi})\boldsymbol{\vartheta}^{(k)}\right] + C\end{aligned} \tag{13}$$

where $\boldsymbol{\Upsilon}^{(k)}$ can be given by

$$\boldsymbol{\Upsilon}^{(k)} \triangleq \mathrm{diag}\left\{\frac{1}{|\vartheta_1^{(k)}|^2+\epsilon},...,\frac{1}{|\vartheta_n^{(k)}|^2+\epsilon},...,\frac{1}{|\vartheta_N^{(k)}|^2+\epsilon}\right\}, \tag{14}$$

$$\boldsymbol{\eta}^{(k)}(\boldsymbol{\varphi}) \triangleq \mathrm{diag}\left\{\eta_1^{(k)}(\varphi_1),...,\eta_m^{(k)}(\varphi_1),...,\eta_M^{(k)}(\varphi_M)\right\}. \tag{15}$$

By exploiting the computational advantage of quadratic optimization, the surrogate function $Q(\boldsymbol{\vartheta},\boldsymbol{\varphi},\boldsymbol{\vartheta}^{(k)})$ is developed, which is more tractable to minimize than the intractable objective function $Q(\boldsymbol{\vartheta},\boldsymbol{\varphi})$. Since

$$\min_{\boldsymbol{\vartheta},\boldsymbol{\varphi}} Q(\boldsymbol{\vartheta},\boldsymbol{\varphi},\boldsymbol{\vartheta}^{(k)}) = \min_{\boldsymbol{\varphi}}\left\{\min_{\boldsymbol{\vartheta}} Q(\boldsymbol{\vartheta},\boldsymbol{\varphi},\boldsymbol{\vartheta}^{(k)})\right\}, \tag{16}$$

By taking the alternative iteration scheme, the optimal solution of the problem $Q(\boldsymbol{\vartheta},\boldsymbol{\varphi},\boldsymbol{\vartheta}^{(k)})$ with respect to (w.r.t.) $\boldsymbol{\vartheta}$ is given by

$$\boldsymbol{\vartheta}^{(k+1)} = \left(\lambda\boldsymbol{\Upsilon}^{(k)} + \boldsymbol{\Phi}^H(\boldsymbol{\varphi})\boldsymbol{\eta}^{(k)}(\boldsymbol{\varphi})\boldsymbol{\Phi}(\boldsymbol{\varphi})\right)^{-1}\boldsymbol{\Phi}^H(\boldsymbol{\varphi})\boldsymbol{\eta}^{(k)}(\boldsymbol{\varphi})\mathbf{z} \tag{17}$$

By replacing $\boldsymbol{\vartheta}$ with $\boldsymbol{\vartheta}^{(k+1)}$ in (16), $\boldsymbol{\varphi}$ can be updated by minimizing the following problem

$$\begin{aligned}\min_{\boldsymbol{\varphi}}\Big\{-\mathbf{z}^H\boldsymbol{\eta}^{(k)}(\boldsymbol{\varphi})\boldsymbol{\Phi}^H(\boldsymbol{\varphi})\Big(&\lambda\boldsymbol{\Upsilon}^{(k)} + \boldsymbol{\Phi}^H(\boldsymbol{\varphi}) \\ &\times\boldsymbol{\eta}^{(k)}(\boldsymbol{\varphi})\boldsymbol{\Phi}(\boldsymbol{\varphi})\Big)^{-1}\boldsymbol{\Phi}^H(\boldsymbol{\varphi})\boldsymbol{\eta}^{(k)}(\boldsymbol{\varphi})\mathbf{z}\Big\}.\end{aligned} \tag{18}$$

It follows that a feasible solution to the problem (18) is highly nonlinear with respect to $\boldsymbol{\varphi}$. To tackle this issue, the proximal projection scheme is exploited to find the next iteration $\boldsymbol{\varphi}^{(k+1)}$, which can be given by

$$\boldsymbol{\varphi}^{(k+1)} = \mathcal{P}_{\mathcal{A}}\left(\mathrm{prox}_{g_\lambda}(\boldsymbol{\varphi}^{(k)} - \nu\nabla G^{(k)}(\boldsymbol{\varphi}^{(k)}))\right), \tag{19}$$

where $\mathcal{P}_{\mathcal{A}}$ denotes the projection onto set $\mathcal{A} \triangleq \{\mathbf{z}^{(k)} | \|\mathbf{z}-$

$\boldsymbol{\Phi}(\boldsymbol{\varphi})\boldsymbol{\vartheta}\|_2 \leq \epsilon\}$, and the gradient $\nabla G^{(k)}(\boldsymbol{\varphi}^k)$ can be readily determined by the chain rule. $\text{prox}_{\mathcal{G}_\lambda}(\cdot)$ is the proximal operator of the function $\mathcal{G}$, which can be used to solve non-convex and non-smooth functions, such as $0 < \ell_p \leq 1$. From [19], the proximal operator can be given by

$$\text{prox}_{g_\lambda}(x) = \begin{cases} \text{sign}(x)(|x| - \lambda), & |x| \leq 2\lambda \\ \dfrac{\text{sign}(x)\sigma\lambda - (1-\sigma)x}{2(\sigma-1)}, & \lambda \leq |x| < \sigma\lambda \\ x, & |x| > \sigma\lambda \end{cases} \tag{20}$$

where σ is constant generally taken as $\sigma > 2$.

By taking the terms (13), (17), and (19), the proposed ℓ_p minimization problem (6) can be solved iteratively to minimize the surrogate function $\boldsymbol{Q}(\boldsymbol{\vartheta}, \boldsymbol{\varphi}, \boldsymbol{\vartheta}^{(k)})$. However, its performance depends on a chosen value of p. To tackle this issue, the global convergence (GC) scheme [20] is developed to determine the feasible value $p^{(k+1)}$, which is derived from

$$\varphi\left(p^{(k)}\right) = \frac{f\left(2p^{(k)}\right)}{f\left(p^{(k)}\right)^2} - \left(p^{(k)} + 1\right), \tag{21}$$

where $f\left(p^{(k)}\right)$ is defined as

$$f\left(p^{(k)}\right) = \mathbb{E}\left\{\left|\varepsilon^{(k+1)}\right|^{p^{(k)}}\right\}, \tag{22}$$

which is the $p^{(k)}$ th order absolute moment of $\varepsilon^{(k+1)}$ and the distribution of $\mathbb{E}\{\cdot\}$ obeys the generalized Gaussian distribution. To obtain the value $p^{(k)}$, the above function can be implemented with the Global Convergence (GC) scheme without look-up table, interpolation, or additional subroutine. Thus, we consider the Newton-Raphson root-finding algorithm on the $\varphi\left(p^{(k)}\right)$ to update the $p^{(k+1)}$, that is

$$p^{(k+1)} = p^{(k)} - \frac{\varphi\left(p^{(k)}\right)}{\varphi'\left(p^{(k)}\right)}, \tag{23}$$

where $\varphi'\left(p^{(k)}\right)$ is the derivative of $\varphi\left(p^{(k)}\right)$ w.r.t. $p^{(k)}$.

On the other hand, the regularization parameter λ is also an important tradeoff between data fidelity and sparsity. In general, a relatively large value λ make a sparse solution, whereas a small value may lead to an underestimation of the frequency components. For this purpose, the heuristic Bayesian approach proposed in [21] is used, where the regularization parameter can be adaptively updated based on the previous iteration. By taking a scaling factor $d > 0$, λ is updated as

$$\lambda^{(k+1)} = \frac{\|\sqrt{\boldsymbol{\eta}^{(k)}(\boldsymbol{\varphi}^{(k)})}\left(\mathbf{z} - \boldsymbol{\Phi}(\boldsymbol{\varphi}^{(k)})\boldsymbol{\vartheta}^{(k)}\right)\|_2^2}{dK} \tag{24}$$

This update rule is based on the value $\sqrt{\boldsymbol{\eta}^{(k)}(\boldsymbol{\varphi}^{(k)})}$, which can contribute to downweight large elements of $\mathbf{z} - \boldsymbol{\Phi}(\boldsymbol{\varphi}^{(k)})\boldsymbol{\vartheta}^{(k)}$. Therefore, the iterative update of λ can be seamlessly inserted into the proposed ℓ_p algorithm for arbitrarily signal-to-noise ratios.

For clarification, the detailed flow chart of the proposed DOA positioning scheme is summarized in Algorithm 1, which is referred to as the robust DOA positioning approximation ℓ_p algorithm. Note that the value of the objective function is gradually decreasing as the number of iterations increases, and then the final solution is solved as $\boldsymbol{\vartheta}$ and $\boldsymbol{\varphi}$. Therefore

Algorithm 1 Robust iteratively approximation ℓ_p algorithm

1: **Initialization**: $\mathbf{z} \in \mathbb{C}^M$; $d > 0$, $\zeta > 0$
2: **Repeat:**
3: **While:** the stopping criterion is not met **do**
4: Update $\boldsymbol{\Upsilon}^{(k)}$ by solving (14);
5: Update $\boldsymbol{\eta}(\boldsymbol{\varphi}^{(k)})$ by solving (15);
6: Update $\boldsymbol{\vartheta}^{(k)}$ by solving (17);
7: Update $\boldsymbol{\theta}^{(k)}$ by solving (19);
8: Update $p^{(k)}$, $\lambda^{(k)}$ by solving (22) and (24);
9: **end while**
10: $k \leftarrow k + 1$
11: **End**
12: **Output** $\boldsymbol{\vartheta}$ and $\boldsymbol{\varphi}$

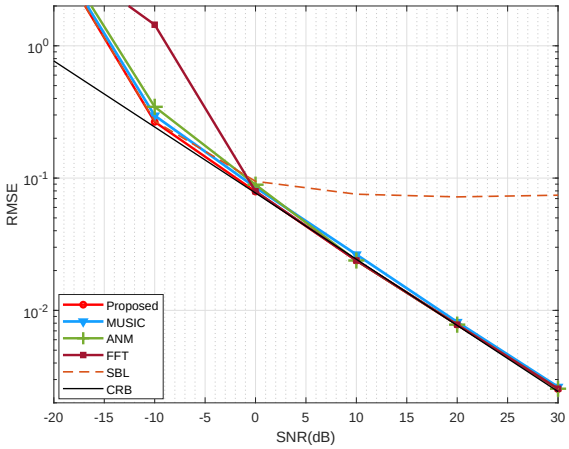

Fig. 2: RMSE performance comparison versus SNR.

it can be easily shown that Algorithm 1 that is monotonically convergent. In the next section, we discuss specific techniques for target localization and their performance.

IV. Simulation Results

In the following, the numerical simulations are provided to evaluate the resolution of the proposed DOA estimation method for the target estimation, and the simulations are carried out in a personal PC with a Intel Core i5-2500K 3.3 GHz processor with 16 GB RAM DDR3. Under these settings, only 2 phases (i.e., 0 and 180°) can be processed at the RIS, where the half wavelength is considered as the distance of the adjacent RIS elements. The carrier frequency is $f_c = 28$ GHz. The root-mean-square error (RMSE) is calculated to validate the estimation result. Multiple measurements instead of receiving channels are adopted to estimate the phase shifts of RIS and DOA. To show the robustness of the proposed estimator, the weighted ℓ_2-norm is adopted instead for comparison . The corresponding Cramér-Rao bound (CRB) for DOA estimation is also derived based on Eq.(5) of [22].

In Fig 2, we first illustrate the DOA estimation resolution with different schemes, where the MUSIC [6], atomic norm minimization (ANM) [12], Sparse Bayesian learning (SBL) [23] and fast Fourier transformation (FFT)-based scheme are included for comparison against the proposed scheme. It is seen that the proposed ℓ_p scheme provides more lower root

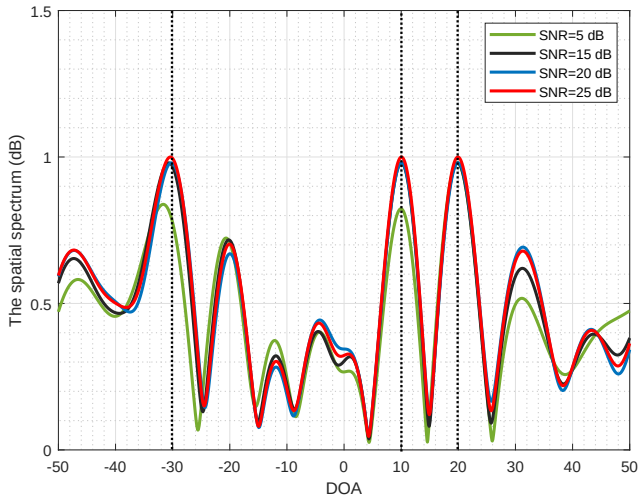

Fig. 3: The spatial spectrum performance comparison vs DOA.

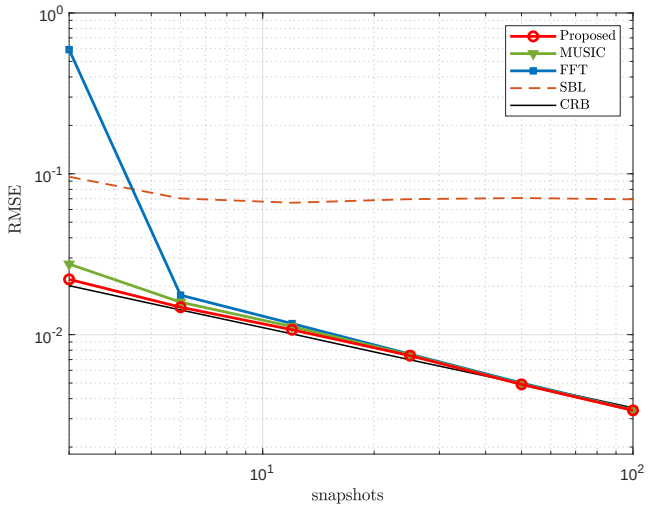

Fig. 4: RMSE performance comparison vs the number of snapshots.

mean squared error (RMSE) value than existing schemes, which confirms the reliability of the proposed ℓ_p estimator, especially with the SNR being lower than 0. The reason is that the estimation accuracy of the proposed ℓ_p estimator can be improved by optimizing the phase shift of RIS, which can obtain the more practical LOS path.

To gain insights into the relationship between spatial spectrum and DOA, Fig. 3 illustrates the spatial spectrum of the proposed ℓ_p method observed with various DOA degree. It can be observed that the estimation error of the proposed estimator is lower than existing estimators, which means that the proposed method has more robust estimation performance to obtain the desired DOA estimation.

Fig. 4 depicts the RMSE performance of different estimators versus the number of snapshots. As seen in Fig. 4, the CRB can be significantly decreased as increasing the number of snapshots. As can be observed that RIS is applied to provide more reflection links, which means that more measurement information can be supplied. On the other hand, the performances of all estimators can be improved with the number of snapshots increasing. In particular, the performance of the proposed ℓ_p scheme is close to the MUSIC algorithm when the number of snapshots is larger than 80, but outperforms those of compared schemes. In addition, the results also show that the proposed estimator has a comparable accuracy with the increasing number of snapshots as expected.

V. Conclusion

The DA-based target positioning has been studied in the RIS-assisted MIMO radar system. Different from the existing methods, the non-convex ℓ_p method was exploited to control of the radar receiver and optimize the the phase shifts of the RIS. Then, the formulated problem was transformed into weighted ℓ_2 approximation, where the reflection coefficients and target DOA were optimized jointly and iteratively until convergence. The efficiency of the proposed estimator is validated in the RIS-assisted positioning simulations using the weighted ℓ_2 approximation. Future work will focus on the multi-RIS target positioning with lower computational complexity and the performance of the DOA estimation.

References

[1] Z. Yu, J. Li, Q. Guo, and J. Ding, "Efficient direct target localization for distributed MIMO radar with expectation propagation and belief propagation," *IEEE Transactions on Signal Processing*, vol. 69, pp. 4055–4068, 2021.

[2] S. Buzzi, E. Grossi, M. Lops, and L. Venturino, "Foundations of MIMO radar detection aided by reconfigurable intelligent surfaces," *IEEE Transactions on Signal Processing*, vol. 70, pp. 1749–1763, 2022.

[3] K. Zhu, Y. Wei, and R. Xu, "TOA-based localization error modeling of distributed MIMO radar for positioning accuracy enhancement," in *2016 CIE International Conference on Radar (RADAR)*, pp. 1–5, 2016.

[4] F. Xu, M. W. Morency, and S. A. Vorobyov, "DOA estimation for transmit beamspace MIMO radar via tensor decomposition with vandermonde factor matrix," *IEEE Transactions on Signal Processing*, vol. 70, pp. 2901–2917, 2022.

[5] A. Hassanien, M. G. Amin, Y. D. Zhang, and F. Ahmad, "High-resolution single-snapshot DOA estimation in MIMO radar with colocated antennas," in *2015 IEEE Radar Conference (RadarCon)*, pp. 1134–1138, 2015.

[6] M. Wagner, Y. Park, and P. Gerstoft, "Gridless DOA estimation and root-MUSIC for non-uniform linear arrays," *IEEE Transactions on Signal Processing*, vol. 69, pp. 2144–2157, 2021.

[7] Z. Wang, L. Qiusheng, X. Zhang, and G. Lixin, "Toeplitz cyclic-MUSIC algorithms for DOA estimation of the SOCS correlated signals," *IEEE Sensors Letters*, vol. 6, no. 11, pp. 1–4, 2022.

[8] Y. Ma, Y. Zeng, and S. Sun, "A deep learning based super resolution DoA estimator with single snapshot MIMO radar data," *IEEE Transactions on Vehicular Technology*, vol. 71, no. 4, pp. 4142–4155, 2022.

[9] M. Rossi, A. M. Haimovich, and Y. C. Eldar, "Spatial compressive sensing for MIMO radar," *IEEE Transactions on Signal Processing*, vol. 62, pp. 419–430, jan 2014.

[10] Z. Chen, G. Chen, J. Tang, S. Zhang, D. K. C. So, O. A. Dobre, K.-K. Wong, and J. Chambers, "Reconfigurable intelligent surface-assisted B5G/6G wireless communications: Challenges, solution and future opportunities," *IEEE Communications Magazine*, pp. 1–7, 2022.

[11] S. Fang, G. Chen, P. Xu, J. Tang, and J. A. Chambers, "SINR maximization for RIS-assisted secure dual-function radar communication systems," in *2021 IEEE Global Communications Conference (GLOBECOM)*, pp. 01–06, 2021.

[12] P. Chen, Z. Yang, Z. Chen, and Z. Guo, "Reconfigurable intelligent surface aided sparse DOA estimation method with non-ULA," *IEEE Signal Processing Letters*, vol. 28, pp. 2023–2027, 2021.

[13] Z. Chen, J. Tang, X. Y. Zhang, D. K. C. So, S. Jin, and K.-K. Wong, "Hybrid evolutionary-based sparse channel estimation for IRS-assisted mmwave MIMO systems," *IEEE Transactions on Wireless Communications*, vol. 21, no. 3, pp. 1586–1601, 2022.

[14] H. Wymeersch, J. He, B. Denis, A. Clemente, and M. Juntti, "Radio localization and mapping with reconfigurable intelligent surfaces: Challenges, opportunities, and research directions," *IEEE Vehicular Technology Magazine*, vol. 15, no. 4, pp. 52–61, 2020.

[15] J. He, H. Wymeersch, T. Sanguanpuak, O. Silven, and M. Juntti, "Adaptive beamforming design for mmwave RIS-aided joint localization and communication," in *2020 IEEE Wireless Communications and Networking Conference Workshops (WCNCW)*, pp. 1–6, 2020.

[16] S. Karimian-Azari, J. R. Jensen, and M. G. Christensen, "Computationally efficient and noise robust DOA and pitch estimation," *IEEE/ACM Transactions on Audio, Speech, and Language Processing*, vol. 24, no. 9, pp. 1613–1625, 2016.

[17] Z. Chen, Y. Fu, Y. Xiang, and R. Rong, "A novel iterative shrinkage algorithm for CS-MRI via adaptive regularization," *IEEE Signal Processing Letters*, vol. 24, no. 10, pp. 1443–1447, 2017.

[18] Z.-Q. He, H. Li, Z.-P. Shi, J. Fang, and L. Huang, "A robust iteratively reweighted ℓ_2 approach for spectral compressed sensing in impulsive noise," *IEEE Signal Processing Letters*, vol. 24, no. 7, pp. 938–942, 2017.

[19] F. Ghayem, M. Sadeghi, M. Babaie-Zadeh, S. Chatterjee, M. Skoglund, and C. Jutten, "Sparse signal recovery using iterative proximal projection," *IEEE Transactions on Signal Processing*, vol. 66, no. 4, pp. 879–894, 2018.

[20] K.-S. Song, "A globally convergent and consistent method for estimating the shape parameter of a generalized gaussian distribution," *IEEE Transactions on Information Theory*, vol. 52, no. 2, pp. 510–527, 2006.

[21] J. Fang, F. Wang, Y. Shen, H. Li, and R. S. Blum, "Super-resolution compressed sensing for line spectral estimation: An iterative reweighted approach," *IEEE Transactions on Signal Processing*, vol. 64, no. 18, pp. 4649–4662, 2016.

[22] P. Stoica, E. Larsson, and A. Gershman, "The stochastic CRB for array processing: a textbook derivation," *IEEE Signal Processing Letters*, vol. 8, no. 5, pp. 148–150, 2001.

[23] K. L. Gemba, S. Nannuru, and P. Gerstoft, "Robust ocean acoustic localization with sparse bayesian learning," *IEEE Journal of Selected Topics in Signal Processing*, vol. 13, no. 1, pp. 49–60, 2019.